Inhibition of Isoprene Biosynthesis Pathway Enzymes by Phosphonates, Bisphosphonates, and Diphosphates

Feng Cheng and Eric Oldfield*

Departments of Chemistry and Biophysics, 600 South Mathews Avenue, University of Illinois at Urbana-Champaign, Urbana, Illinois 61801

Received February 13, 2004

We have investigated the docking of a variety of inhibitors and substrates to the isoprene biosynthesis pathway enzymes farnesyl diphosphate synthase (FPPS), isopentenyl diphosphate/dimethylallyl diphosphate isomerase (IPPI) and deoxyxylulose-5-phosphate reductoisomerase (DXR) using the Lamarckian genetic alogorithm program, AutoDock. The docked ligand structures are predicted with a ∼0.8 Å rms deviation from the structures determined crystallographically. The errors found are a function of the number of atoms in the ligand ($R = 0.91$, $p < 0.0001$) and, to a lesser extent, on the resolution of the crystallographic structure ($R = 0.70$, $p < 0.008$). The structures of three isoprenoid diphosphates docked to the FPPS enzyme reveal strong electrostatic interactions with Mg^{2+}, lysine and arginine active site residues. Similar results are obtained with the docking of four IPPI inhibitors to the IPPI enzyme. The DXR substrate, deoxyxylulose-5-phosphate, is found to dock to Mn^{2+}−NADPH−DXR in an almost identical manner as does the inhibitor fosimdomycin to Mn^{2+}−DXR (ligand heavy atom rms deviation = 0.90 Å) and is poised to interact with NADPH. Bisphosphonate inhibitors are found to bind to the allylic binding sites in both eukaryotic and prokaryotic FPPSs, in good accord with recent crystallographic results (a 0.4 Å rms deviation from the X-ray structure with the *E. coli* enzyme). Overall, these results show for the first time that the geometries of a broad variety of phosphorus-containing inhibitors and substrates of isoprene biosynthesis pathway enzymes can be well predicted by using computational methods, which can be expected to facilitate the design of novel inhibitors of these enzymes.

Introduction

Inhibitors of enzymes involved with the biosynthesis of isoprenoid lipids are currently of great interest in the context of the treatment of bone resorption diseases, infectious diseases and cancer.[1−7] For example, the bisphosphonate class of ligands, such as pamidronate (Aredia) **1**, alendronate (Fosamax) **2**, risedronate (Actonel) **3**, and zoledronate (Zometa) **4** are potent inhibitors of the enzyme farnesyl diphosphate synthase (FPPS).

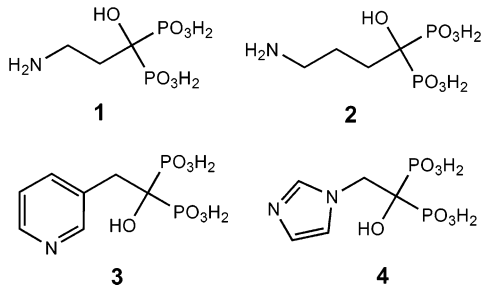

They are used extensively in the treatment of osteoporosis, Paget's disease, and hypercalcemia due to malignancy and make a ∼5 billion dollar contribution to the global pharmaceutical market. These compounds have also been found to have antiparasitic activity, with parasitological cures of both cutaneous and visceral leishmaniasis having been reported.[3,4] Bisphosphonates also stimulate the $\gamma\delta$ T cells of the immune system and such activated T cells have both anticancer[5,6] and antibacterial[7] activity. Another class of phosphorus-containing compounds, diphosphates, are inhibitors of the mevalonate/isoprene biosynthesis pathway enzyme isopentenyl diphosphate/dimethylallyl diphosphate isomerase (IPPI[8−10]), and yet another class of compounds, monophosphonates, are inhibitors of the nonmevalonate or deoxyxylulose-5-phosphate (DXP) pathway for isoprenoid biosynthesis[11] and have considerable potential as antimalarial drugs.[12] The crystallographic structures of several diphosphates bound to FPPS and IPPI have been reported,[9,10,13] as has the structure of the phosphonate, fosmidomycin, bound to deoxyxylulose-5-phosphate reductoisomerase (DXR[14]). However, nothing is known crystallographically about how the bisphosphonate drugs bind to *eukaryotic* FPPSs, although recently the structure of a ternary *prokaryotic* FPPS−risedronate−IPP complex has been reported.[15] We have therefore investigated the docking of a broad range of phosphate and phosphonate species to FPPS, IPPI and DXR, to see to what extent it is possible to predict their bound conformations, using the Lamarckian genetic algorithm program, AutoDock,[16] to provide a basis for the design of other, novel inhibitors.

Computational Aspects. Protein structures (PDB files 1UBW, 1UBX, 1UBY, 1Q54, 1NFS, 1R67, 1ONP, 1PPW and the two ternary complexes of *E. coli* FPPS

* To whom correspondence should be addressed. E-mail: eo@chad.scs.uiuc.edu.

10.1021/jm040036s CCC: $27.50
Published on Web 09/10/2004

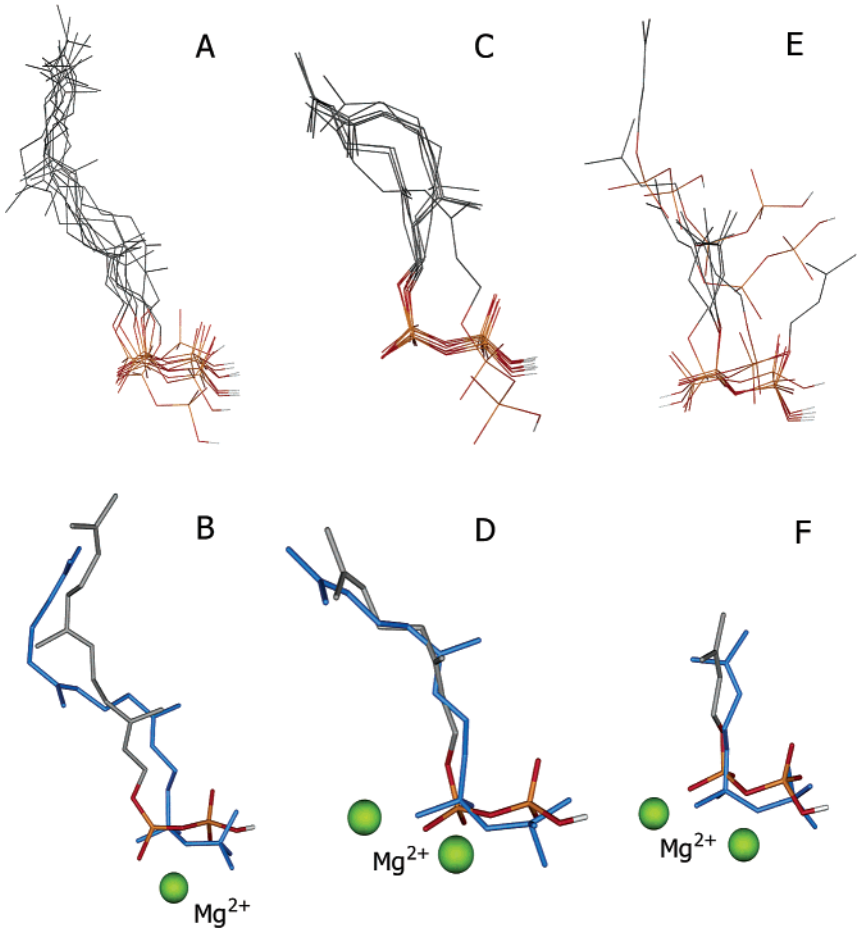

Figure 1. Docking of diphosphate ligands to FPPS. A, FPP, 10 lowest energy conformations. B, The lowest energy conformation of FPP plus (in blue) the X-ray structure (PDB file 1UBX). C, GPP, 10 lowest energy conformations. D, The lowest energy conformation of GPP plus (in blue) the X-ray structure (PDB file 1UBW). E, DMAPP, 10 lowest energy conformations. F, The lowest energy conformation of DMAPP plus (in blue) the X-ray structure (1UBY). The RMS errors between the lowest energy conformations and the X-ray structures are 1.61 Å (B), 1.37 Å (D) and 0.85 Å (F).

kindly provided by D. Hosfield, PDB files 1RQJ and 1RQI) were prepared by using the molecular modeling program SYBYL 6.9.[17] All waters were removed, polar hydrogen atoms added geometrically and Kollman united-atom partial charges[18] assigned. The diphosphates (and bisphosphonates) were assigned two negative charges, the phosphonate and hydroxamate groups in fosmidomycin a single negative charge each. Metal ions (Mg^{2+}, Mn^{2+}) were retained and their charges both assigned as +2.0. The properties of the protein's active site were represented with atomic affinity grids.[16] In all cases, we used grid maps having 61 × 61 × 61 points with a grid-point spacing of 0.375 Å.[16] This ensures that the boxes containing the affinity grids are of sufficient size (22.5 Å × 22.5 Å × 22.5 Å) to include the entire active site, as well as providing enough space for translation and rotation of the ligands. The grids were generally centered on the ligand of interest. The initial structures of the ligands were generated using SYBYL 6.9 in the all atom representation, that is, all hydrogens were added explicitly. Ligand atomic charges were calculated by using the Gasteiger−Marsili method.[19] The geometries of these compounds were then optimized by using the Tripos force field.[20] The AutoDock 3.0 software package,[16] which uses a Lamarckian genetic algorithm, was used for all molecular docking simulations. Each simulation was performed 50 times, yielding 50 docked conformations. The genetic algorithm parameters for docking were as follows: population size = 50; mutation rate = 0.02 and crossover rate = 0.8. Simulations were performed using up to 2.5 million energy evaluations with a maximum of 27 000 generations. The number of generations for picking the worst individual conformation (ga_window_size) was set to 10. All calculations were performed on a Silicon Graphics (Mountain View, CA) Fuel R14000 workstation.

Results and Discussion

We first investigated the docking of diphosphates to FPPS and IPPI, followed by docking of the phosphonate inhibitor, fosmidomycin, to DXR. In all cases, crystallographic structures were known, so these calculations provide a good test of the accuracy of the method with these enzymes and substrates or inhibitors, setting the stage for additional studies on systems whose structures are not yet known. We show in Figure 1 the results of docking farnesyl diphosphate (FPP, **5**, Figure 1A,B), geranyl diphosphate (GPP, **6**, Figure 1C,D) and dimethylallyl diphosphate (DMAPP, **7**, Figure 1E,F) to a mutant avian FPP synthase (PDB files 1UBX, 1UBW and 1UBY, respectively).

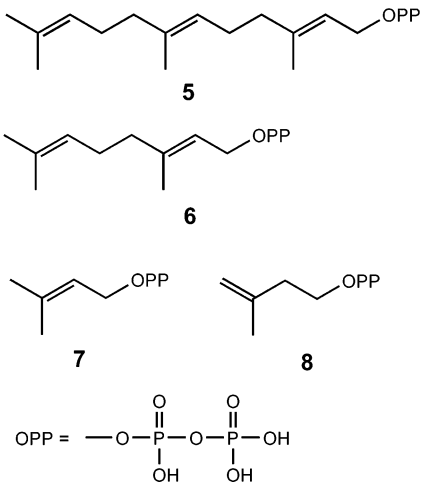

The binding of FPP (the product of the FPP synthase reaction) is relatively challenging in that FPP contains 50 atoms connected by 10 rotatable bonds (Table 1) and when fully extended is ~19.5 Å long. Nevertheless, the docked conformations follow closely the bound FPP structure found crystallographically,[13] as shown in Figure 1. The structures of the 10 lowest energy structures found are shown in Figure 1A and the single lowest energy structure is shown in Figure 1B, together with the crystallographic result (shown in blue), where there is a 1.61 Å rms deviation for the heavy atoms from the structure determined crystallographically. The diphosphate moiety is found to bind to the Mg^{2+} found crystallographically, and is also stabilized by electrostatic interactions with active site arginine and lysine residues. Similar good accord is found with the GPP and DMAPP structures, Figure 1C−F, with errors of 1.37 Å and 0.85 Å being observed for the lowest energy conformations, Table 1. Of particular note is that the ligand curvature seen crystallographically with FPP and GPP is clearly reproduced in these simulations, Figures 1B and 1D.

We next investigated the docking of a series of diphosphate inhibitors of the isopentenyl diphosphate/dimethylallyl diphosphate isomerase enzyme. These inhibitors are all analogues of the substrates DMAPP (**7**) and isopentenyl diphosphate (IPP, **8**) and have the following structures:

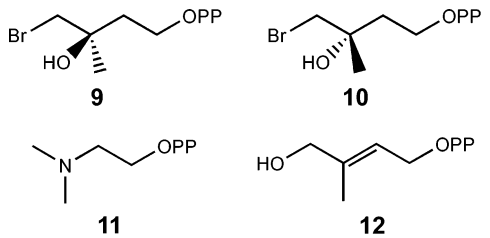

Compounds **9** and **10** are the (chiral) bromohydrin adducts of IPP, **11** is the azadihydro analogue of IPP (dimethylaminoethyl diphosphate, DMAEPP) and **12** is *E*-4-hydroxy-3-methyl-but-2-enyl diphosphate (HMBPP), i.e., hydroxy-DMAPP. The structures of all species bound to either a C67A mutant of IPPI (**9**, **10**) or wt IPPI (**11**, **12**) have been determined crystallographically at between 1.93 and 2.21 Å resolution.[9,10,21] The results presented in Figure 2 show the 10 lowest energy conformations of **9**−**12** bound to IPPI (**A**, **C**, **E** and **G**), together with the single lowest energy conformers (**B**, **D**, **F** and **H**) and for comparison (in blue), the crystallographic results. The rms deviations found for both the A-chain and B-chain results (not shown in Figure 2) are presented in Table 1 and vary between 0.57 and 0.89 Å, for the eight structures. This is clearly an improvement over the results obtained with FPPS and, as shown below, correlates with the smaller number of atoms in the IPPI inhibitors. In all cases, the diphosphate moieties of the ligands are involved in bidentate chelation to the active site Mg^{2+} seen crystallographically, while the distal ends of the ligands are involved in hydrogen-bond or electrostatic interactions with polar, active site amino acids.

The third test system investigated was the phosphonate inhibitor of DXR, fosmidomycin (**13**):

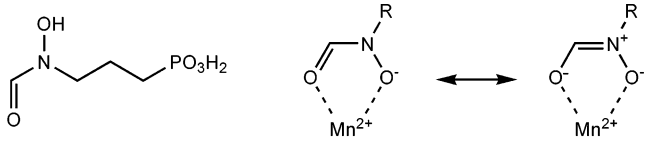

The DXR enzyme contains Mn^{2+}, but in this case the inhibitor does not bind to the metal site via its phosphorus-containing group, as found with the diphosphates binding to FPPS and IPPI, which bind to Mg^{2+}. Rather, the hydroxamate group is involved in forming a strong, bidentate chelate to Mn^{2+}, basically as shown above in **14**, with the phosphonate group being involved in electrostatic/hydrogen bond interactions with lysine, asparagine and serine side chains.[14] Crystal structures of DXR have been reported with either $NADP^+$ bound[22] or with **13** (plus Mn^{2+}).[14] We docked **13** into the Mn^{2+} structure and obtained the results shown in Figures 3A,B. In this case, the rms deviation from the 2.5 Å crystal structure is very small, 0.42 Å, consistent with the small number of total atoms and rotatable bonds, Table 1. The results shown in Figure 3 are of interest since we find little evidence for the docking of any "rotated" fosmidomycin molecules, having their phosphonate groups bound to Mn^{2+} (only 1 of 50 molecules bound this way and this conformer was ranked 20th out of 50, energetically). The reason for this is likely due to the fact that *both* oxygens in the hydroxamate bind to Mn^{2+}, forming a stable, five-membered ring. However, for the phosphonate to form a bidentate chelate,

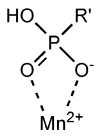

a highly strained four-membered ring would form and this seems energetically unlikely, and of course **14** is in fact the structure seen experimentally.

The results shown in Figures 1−3 and Table 1 indicate that it is possible to predict, with good accuracy, the bound conformations of the diphosphate substrates of FPPS and the diphosphate inhibitors of IPPI, as well as the phosphonate inhibitor of DXR. As can be seen in Figure 4, the rms deviations between the predicted and experimental structures observed are somewhat dependent on the crystallographic resolution (Figure 4A;

Table 1. Docking and Structural Parameters for Phosphate and Phosphonate Ligands Bound to Isoprenoid Pathway Enzymes

protein	PDB file	ligand	RMSD (Å)[a]	RMSD (Å)[b]	N_{rot}[c]	resolution (Å)	N_{atoms}[d]
FPPS	1UBX	FPP (**5**)	1.61	1.80	10	2.50	50
FPPS	1UBW	GPP (**6**)	1.37	1.74	7	2.50	37
FPPS	1UBY	DMAPP (**7**)	0.85	1.12	4	2.40	24
IPPI	1Q54, chain A	*R*-bromohydrin (**9**)	0.73	0.85	7	1.93	27
IPPI	1Q54, chain B	*R*-bromohydrin (**9**)	0.80	0.91	7	1.93	27
IPPI	1Q54, chain A	*S*-bromohydrin (**10**)	0.67	0.74	7	1.93	27
IPPI	1Q54, chain B	*S*-bromohydrin (**10**)	0.64	0.72	7	1.93	27
IPPI	1NFS, chain A	DMAEPP (**11**)	0.62	0.61	5	1.96	26
IPPI	1NFS, chain B	DMAEPP (**11**)	0.57	0.56	5	1.96	26
IPPI	1PPW, chain A	HMBPP (**12**)	0.89	0.91	6	2.21	25
IPPI	1PPW, chain B	HMBPP (**12**)	0.74	0.77	6	2.21	25
DXR	1ONP	fosmidomycin (**13**)	0.42	0.44	4	2.50	19
		mean (SD)	0.83 (±0.34)	0.93 (±0.43)			

[a] The rms deviation in Å between the lowest energy AutoDock conformation and that found crystallographically. [b] The average rms deviation for all top 10 structures. [c] The number of rotatable bonds in the ligand. [d] The number of atoms in the ligand.

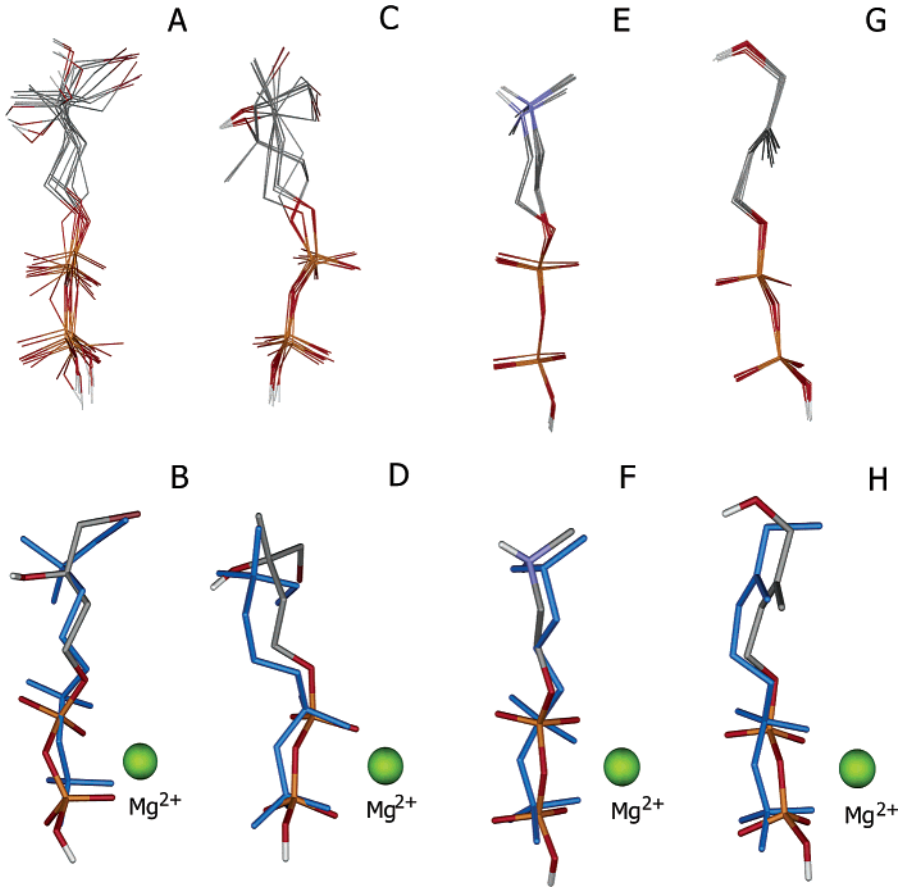

Figure 2. Docking of diphosphate inhibitors to IPPI. A and B show the 10 lowest and single lowest energy conformations of **9** bound to the A chain of 1Q54. The X-ray result is shown in blue. C and D show the equivalent results for **10**. E and F show the equivalent results for **11** bound to 1NFS. G and H show equivalent results for **12** bound to 1PPW. The rms deviations between the lowest energy conformations and the X-ray structures are 0.73 Å (B), 0.67 Å (D), 0.62 Å (E) and 0.89 Å (G). All of the diphosphate moieties are involved in bidentate chelation to Mg^{2+}, and electrostatic interactions with active site arginine and lysine residues.

$R = 0.7$, $p < 0.008$) but are are a much stronger function of the total number of atoms in the inhibitor (Figure 4B, $R = 0.92$, $p < 0.0001$). These results serve as important tests of the use of the AutoDock method to accurately predict the bound conformations of diphosphate and phosphonate inhibitors or substrates of these enzymes having known structures and consequently, in the use of this approach to investigate in more detail the mechanisms of action of FPPS and DXR, as well as the inhibition of eukaryotic FPPSs by bisphosphonate drugs, where the bound conformations are not yet known. However, there is always the possibility that these results might be biased since the protein targets used were prepared simply by removing the ligands of interest. That is, "self-docking" might be much more successful than docking to a broad range of other, related structures. Plus, the use of rms errors to assess validity is only one measure of accuracy. We thus carried out two further sets of calculations. In the first, Figure 5, we made a comparison between the ligand structures seen crystallographically and those computed by using Autodock, simply by counting the number of ligand−protein interactions identified by using the Ligplot[23] program. For the top scoring conformations, we found $R^2 = 0.77$ for the crystal versus Autodock predictions (● symbols in Figure 5), a value which

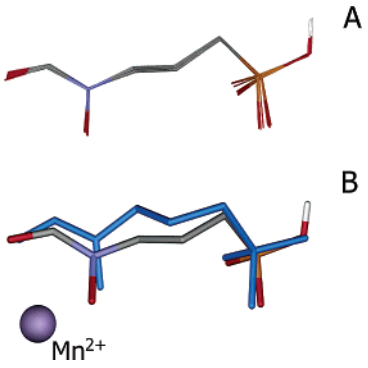

Figure 3. Docking of the phosphonate inhibitor fosmidomycin (**13**) to DXR (PDB file 1ONP). A, 10 lowest energy conformations and B, the single lowest energy conformation. The X-ray result is shown (in blue) in B. The rms deviation between the lowest energy conformation and the X-ray structure is 0.42 Å. With fosmidomycin, the hydroxamate group binds to the divalent metal cation (Mn^{2+}) while the phosphonate is stabilized by electrostatic interactions with lysine and serine residues.

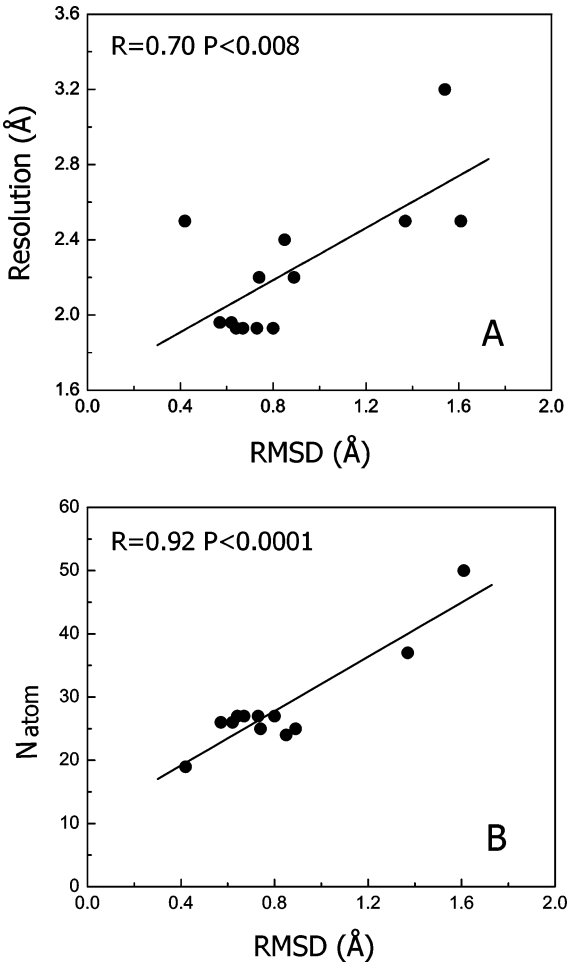

Figure 4. Graphs showing correlations between the rms deviations (in Å) between the docked structures and the crystallographic results. A, correlation between the rms deviation and the crystallographic resolution ($R = 0.70$, $p < 0.008$). B, correlation between the rms deviation and the number of ligand atoms, N_{atoms} ($R = 0.92$, $p < 0.0001$). Data from Table 1.

decreased to $R^2 = 0.39$ when all top 10 scoring Autodock structures were employed (○ symbols in Figure 5), in accord with the results obtained by using rms deviations (Table 1).

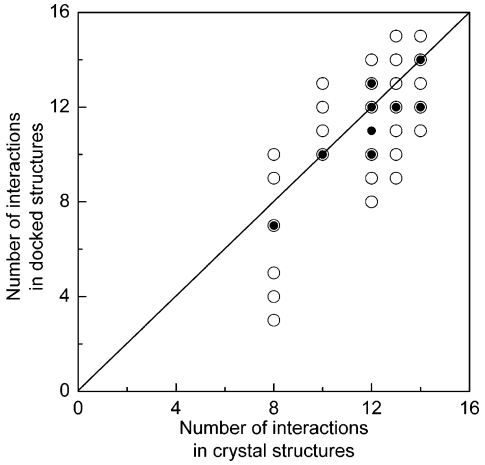

Figure 5. Graph showing correlation between number of Ligplot[23] interactions found in crystal structures and Autodock[16] structures. ● = top scoring conformation; ○ = next 9 top scoring conformation. The structures investigated are those in Table 1.

To investigate the question of self-docking bias, we next carried out a series of cross-docking experiments in which ligands were docked via Autodock to other, related crystal structures. The results of these cross-docking calculations are shown in Table 2, for FPP and IPPI, where multiple structures have been reported. For FPPS, we found generally good accord between experiment and the Autodock results using PDB Files 1UBV, 1UBY, 1UBW and 1UBX, but there was relatively poor agreement for DMAPP (the smallest ligand) binding to the FPP bound structure (1UBX), indicating most likely small conformational differences between the DMAPP and FPP bound protein structures. The presence of Mg^{2+} was found to be essential for ligand binding, with rms errors of ~3.8 Å being found with 1UBV lacking Mg^{2+}, Table 2. For the binding of **9**−**12** to IPPI (PDB structures 1Q54, INFS and 1PPW) there was, as expected, a small bias toward the "self-docked" structure, Table 2, although overall the results of the cross-docking calculations were quite good (a 1.08 Å error for cross-docking versus 0.70 Å for self-docking).

We next considered the inhibition of FPPS by the bisphosphonate bone resorption drugs, risedronate (**3**) and minodronate (**15**), whose structure is shown below:

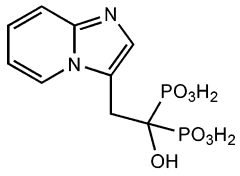

15

Both are potent inhibitors of an expressed, recombinant human FPPS,[24] and **3** is a potent inhibitor of FPPSs from *Trypanosoma cruzi*,[25] *T. brucei*[26] and *Leishmania major*.[27] It is known that FPPS inhibition by bisphosphonates such as **3** (and **2**) is competitive with respect to allylic pyrophosphate substrates (such as GPP), but is not competitive with respect to the homoallylic substrate IPP, implying that biphosphonates act as allylic pyrophosphate analogues, binding to the GPP (or DMAPP) site.[28] As with our previous quantita-

Table 2. Results of Cross-Docking Calculations on FPPS and IPPI

structure	docked ligand		
	DMAPP (**7**) (RMSD, Å)	GPP (**6**) (RMSD, Å)	FPP (**5**) (RMSD, Å)
1UBV (without Mg)	4.31	3.72	3.48
1UBV (Mg)	1.11	1.49	1.73
1UBY (DMAPP)	0.85	1.47	1.78
1UBW (GPP)	0.99	1.37	1.35
1UBX (FPP)	1.68	1.94	1.61

structure	docked ligand			
	R-bromohydrin (**9**) (RMSD, Å)	*S*-bromohydrin (**10**) (RMSD, Å)	DMAEPP (**11**) (RMSD, Å)	HMBPP (**12**) (RMSD, Å)
1Q54 chain A	0.73	0.67	0.88	1.30
1Q54 chain B	0.80	0.64	0.93	1.07
1NFS chain A	1.05	0.94	0.62	1.29
1NFS chain B	1.46	1.57	0.57	1.14
1PPW chain A	1.48	0.94	0.73	0.89
1PPW chain B	1.04	1.26	0.92	0.74

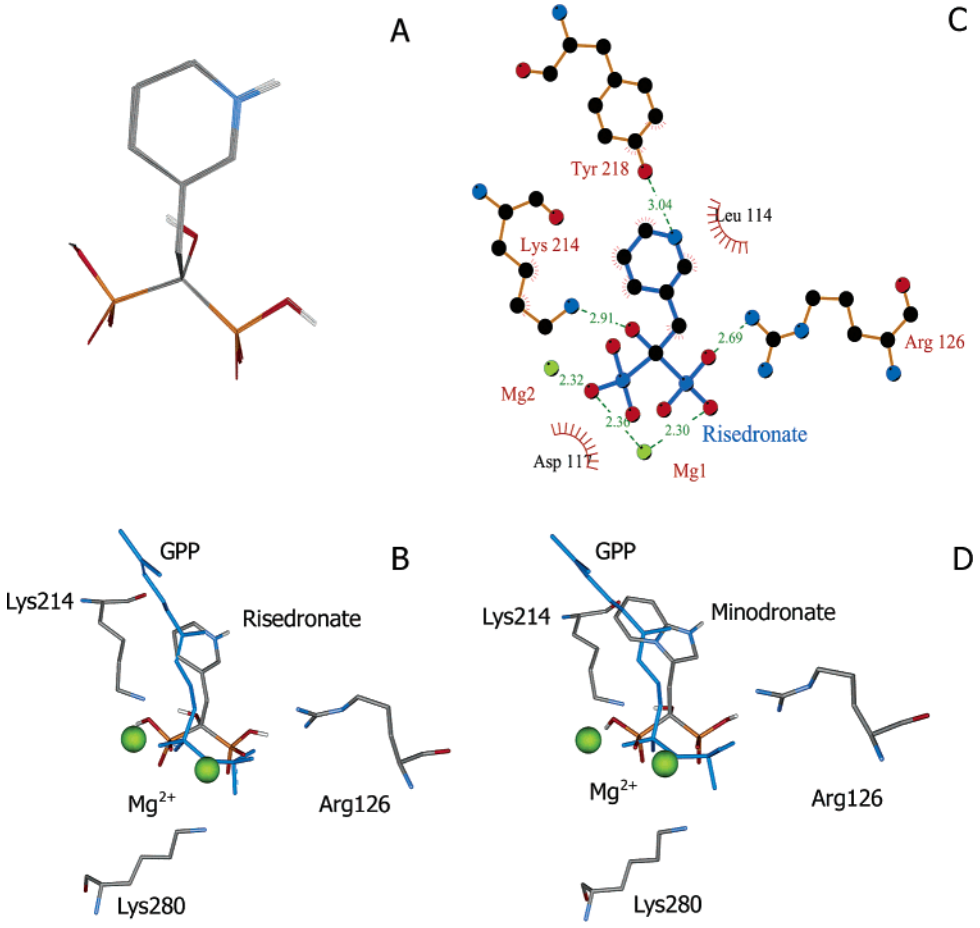

Figure 6. Docked structures and Ligplot[23] interactions between bisphosphonate inhibitors and an avian FPPS. A, Risedronate, 10 lowest energy conformations. B, Risedronate, the lowest energy conformation together with (in blue) the X-ray result for GPP (PDB file 1UBW). Also shown are selected active site residues involved in diphosphate stabilization. C, Ligplot[23] diagram showing the main interactions between risedronate and FPPS. D, Lowest energy conformer of minodronate together with (in blue) the X-ray results for GPP bound to FPPS.

tive structure−activity relationship investigations of bisphosphonate inhibition of FPPS[27] and growth inhibition (mediated via FPPS inhibition) of *T. brucei*,[29] bone resorption[30] and $\gamma\delta$ T cell activation,[31] we used molecules having protonated side-chains, together with monoanionic phosphonate groups (based on our previous QSAR and crystallographic studies;[27,32]). Figure 6A shows the 10 lowest energy structures found for risedronate (**3**) and Figure 6B, the single lowest energy conformer, together with for comparison (in blue) the structure of GPP bound to FPPS.[13] As may be seen in Figure 6, the bound risedronate structure docks to FPPS in basically the same manner as does GPP. Figure 6C shows in more detail the specific intermolecular contacts in the form of a Ligplot[23] diagram, which indicates that the phosphonate groups are involved in electrostatic interactions with Mg_1 and Mg_2, plus, they are stabilized by electrostatic interactions with K214 and R126. There

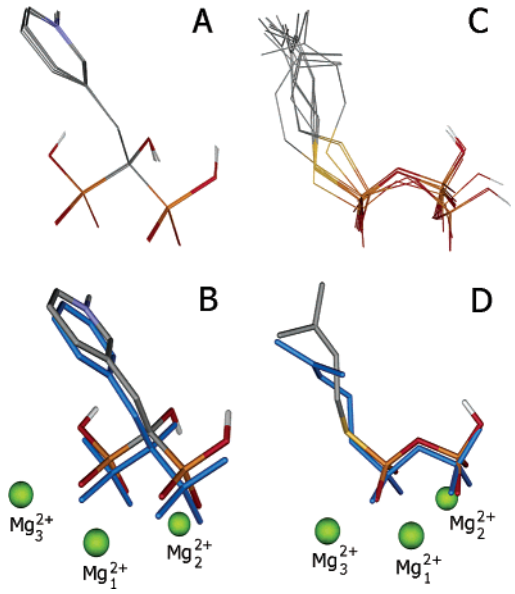

Figure 7. Docked structures of risedronate (**3**) and DMSPP bound to an *E. coli* FPPS−IPP complex. A, risedronate, 10 lowest energy conformations. B, risedronate, lowest energy conformation with (in blue) the X-ray result. C, DMSPP, 10 lowest energy conformations. D, DMSPP, lowest energy conformation with (in blue) the X-ray result. The rms deviations between the predicted and crystallographic structures are 0.40 Å (risedronate) and 1.04 Å (DMSPP).

is also a hydrogen bond between the pyridium group of risedronate and the OH group of Y218. The pyridinium group is placed in about the same position as the putative carbocation transition state/reactive intermediate predicted earlier,[33] based on purely manual docking of **3** into the active site of FPPS.

Similar results are found with minodronate (**15**), Figure 6D. The larger, fused ring structure of **15** might be expected to dock with even more accuracy than with **3**, since there are more opportunities for repulsive interactions with the protein, as well as enhanced hydrophobic interactions, while the number of rotational degrees of freedom remain the same. As may be seen in Figure 6D, **15** docks in essentially the same manner as does **3**, with electrostatic interaction with Mg, R126, K214 and, K280. The aromatic rings of both **3** and **15** are also involved in hydrophobic contacts with the protein. These results are of interest since they confirm the idea discussed previously,[33] that bisphosphonates can bind into the allylic site of FPPS with their phosphonates binding to Mg^{2+}, lysine and arginine residues, while the aromatic rings are involved with hydrogen bonding (electrostatic), as well as hydrophobic, interactions with the protein.

Interestingly, shortly after we completed these docking investigations, Hosfield et al.[15] reported the crystallographic structures of two FPPS inhibitors, risedronate and dimethylallyl *S*-thiolodiphosphate (DMSPP), bound to a *prokaryotic* FPPS containing IPP,[15] prompting us to investigate the binding of these inhibitors to FPPS, with particular interest in testing the predictions we made above on risedronate binding. The eukaryotic and prokaryotic FPPSs have considerable sequence differences toward the C-terminus, but the two key DDXX-(XX)D motifs are still present. The results of the docking calculations are shown in Figures 7A,B for risedronate

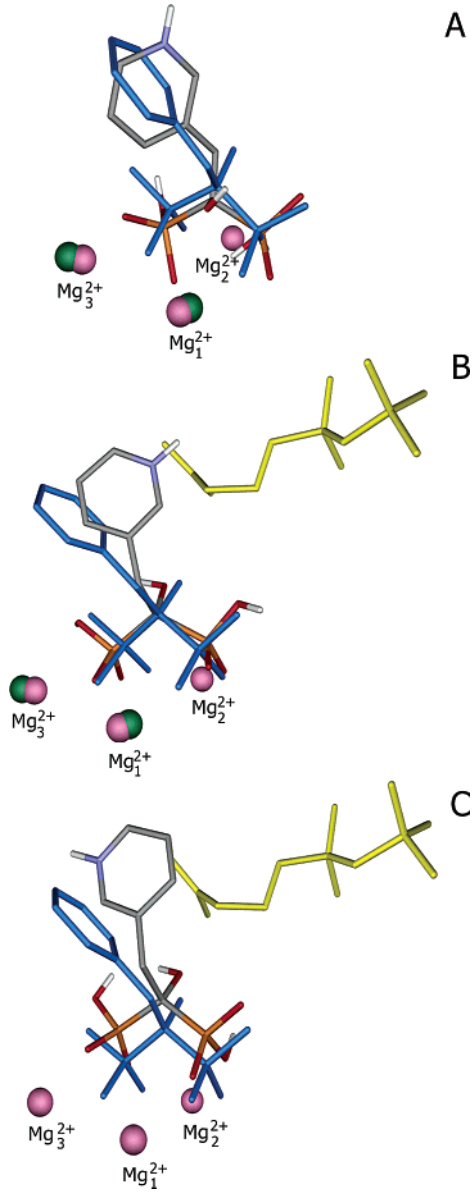

Figure 8. Comparisons between predicted and experimental risedronate conformations. A, Binary risedronate/avian FPPS structure[33] and in blue, X-ray conformation in ternary IPPI−risedronate *E. coli* complex.[15] B, as A but binary avian Autodock structure. The location or IPP in the ternary complex is shown in yellow. C, Autodock structure of risedronate bound to the X-ray structure in the absence of IPP. The Mg^{2+} in the risedronate−FPPS−IPP X-ray structure are shown in pink, those in the avian GPP−FPPS structure used for docking, in green.

and in Figure 7C,D, for DMSPP, docked to the *E. coli* FPPS−IPP complex (obtained in each case by removal of the inhibitor from the reported crystallographic structures). Once again, we find the lowest energy docked structures (Figures 7B,D) to be in good agreement with the crystallographic results (shown in blue), with 0.40 Å (risedronate) and 1.04 Å (DMSPP) rms deviations being found.

The availability of these new crystal structures now permits us to probe in more detail a number of interesting questions about the interactions of risedronate with FPPS. For example: how similar is the bound risedronate structure to that predicted earlier (in the binary, eukaryotic FPPS complex) and the binary structure

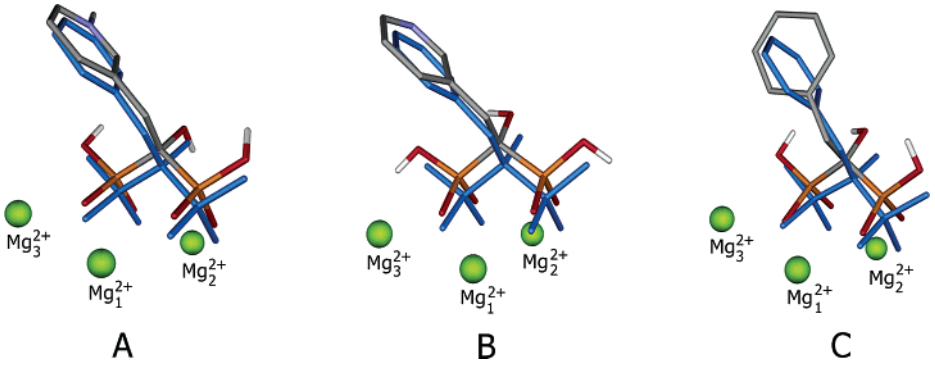

Figure 9. Comparison between Autodock structures of A, risedronate (pyridinium form); B, risedronate (pyridine form) and C de-aza risedronate, docked to the *E coli* structure (+IPP), superimposed on the X-ray structure (in blue).

discussed above? How important are each of the three Mg^{2+} in risedronate binding? How does IPP affect risedronate binding? How important are electrostatic vs hydrophobic interactions between the bisphosphonate side chains and the protein? To begin with, we compare the structure of risedronate proposed earlier[33] with that now found (in the ternary complex with IPP), as shown in Figure 8A. The two FPPS structures were aligned by using the Biopolymers Align module in the Sybyl program. There is a 1.28 Å rms deviation between the two structures, primarily due to the uncertainty in the C_1−OH position (up or down) in the original structure proposed. The Mg^{2+} in the reference *E. coli* risedronate-FPPS−IPP structure are shown in pink (Mg_1−Mg_3), those in the avian FPP−FPPS structure used for docking, in green. With the Autodock, binary, avian predicted structure, Figure 8B, the rms error is even larger (1.34 Å), due to the presence of IPP in the ternary (*E. coli*) complex, which constrains side chain movement in risedronate, and as shown in Figure 7B, the rms error found when using the IPP-bound *E. coli* FPPS is only 0.40 Å. Removal of IPP from the ternary *E. coli* complex also results in poor risedronate docking, Figure 8C, with an rms error of 1.99 Å.

The actual charge on the aromatic ring also influences the docked conformation, as shown in Figure 9. With the pyridinium (protonated) form of risedronate, as noted above, there is excellent accord between the crystal structure and that predicted, as reproduced in Figure 9A. However, on deprotonation of the pyridinium group, the rms error increases from 0.40 to 0.62 Å (Figure 9B) and with a de-aza (i.e. a phenyl) analogue of risedronate, the error increases further, to 1.12 Å, Figure 9C. These results strongly suggest the importance of having a protonated side chain capable of undergoing electrostatic interactions in the protein and are consistent with the observation that all potent bisphosphonate inhibitors of FPPS have such basic side chains. For example, risedronate has a K_i of 16 nM while the phenyl analogue has an IC_{50} of 1.6 μM, against a *L. major* FPPS,[27] since there can be no significant hydrogen bonding or other electrostatic interaction with the benzene ring.

The availability of the ternary complex structure is also of interest since it contains three Mg^{2+}, raising the question as to which ones are most important in risedronate binding. To investigate this question, we docked risedronate (pyridinium form) to the ternary complex FPPS structure, without and with IPP, and in the presence of 0, 1, 2 or 3 Mg^{2+}. As may be seen in Table 3, all docked structures for the IPP-free protein gave poor accord with experiment, due to movement of the risedronate side chain into the region normally occupied by IPP. However, in the presence of IPP, as noted above, excellent accord was found with all three Mg^{2+} present, and the next three best structures all contained Mg_1, which therefore appears to be of particular importance in risedronate binding, Table 3. This Mg is involved in bidentate chelation to both P_1 and P_2, Figures 7 and 9, and is in essentially the same position as that involved with bidentate chelation with diphosphate in the FPPS−substrate complexes.

Table 3. Results of Docking Risedronate (**3**) to an *E. coli* FPPS in the Presence or Absence of IPP (**8**) and with Variable Mg^{2+} Loadings

number of Mg^{2+}	Mg_1	Mg_2	Mg_3	rmsd (Å)
		With IPP		
0	0	0	0	5.57
1	0	0	1	4.93
	0	1	0	1.93
	1	0	0	1.69
2	1	1	0	1.71
	1	0	1	1.69
	0	1	1	2.14
3	1	1	1	0.40
		No IPP		
0	0	0	0	3.29
1	0	0	1	3.32
	0	1	0	4.27
	1	0	0	3.25
2	1	1	0	2.44
	1	0	1	2.40
	0	1	1	2.09
3	1	1	1	1.99

Finally, we consider the docking of deoxyxylulose-5-phosphate **16** (DXP): to deoxyxylulose-5-phosphate reductoisomerase (DXR). In this case, the conformation of the bound substrate in the NADPH-loaded enzyme is not known, in any system. We used Sybyl 6.9 to convert $NADP^+$−DXR[22] to the NADPH form, then used Autodock to dock the DXP substrate. The docked conformation results for DXP are shown in Figures 10A,B where the 10 lowest energy (Figure 10A) and the

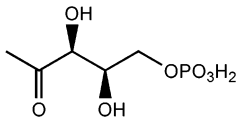

16

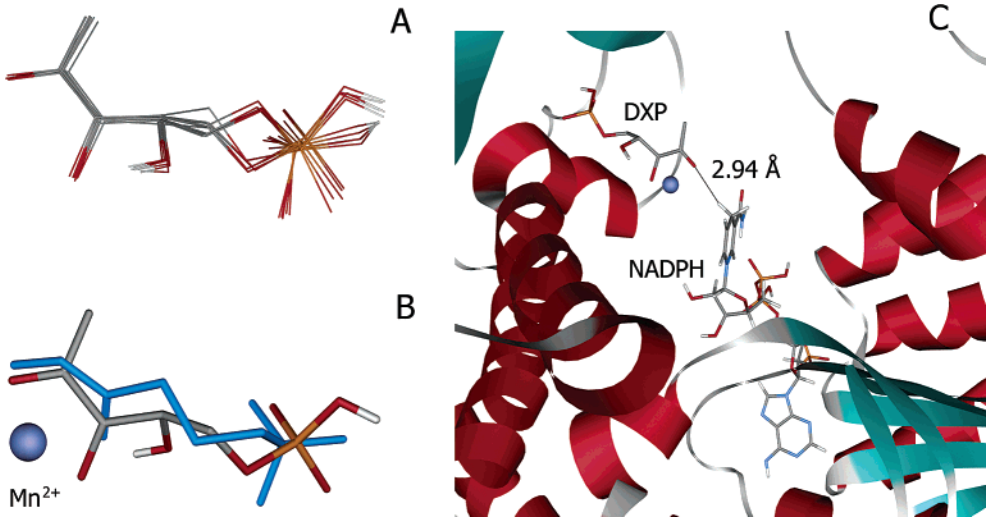

Figure 10. Docked structures of deoxyxylulose-5-phosphate (**16**) bound to NADPH−DXR. A, 10 lowest energy conformations. B, Comparison between the docked conformation of DXP (**16**) and the crystallographic structure (in blue) of fosmidomycin (**13**) bound to DXR. The rms deviation between the heavy atoms is 0.90 Å. C, Docked structure of DXP (**10**) bound to an NADPH−DXR structure (based on an alignment of PDB files 1JVS and 1ONP).

single lowest energy (Figure 10B) conformers are compared with the crystallographic result found for fosmidomycin (in blue), Figure 10B.[14] The heavy atom backbone and phosphate/phosphonate rms deviation between the docked DXP and the crystallographic result for fosmidomycin ($N = 11$ atoms) is 0.90 Å. The docking results also reveal a ∼2.9 Å distance between the carbonyl oxygen (O1) of DXP and H_s of NADPH, Figure 10C, in general accord with the modeling results reported by Steinbacher et al.[14]

Conclusions

The results we have presented above are of interest for a number of reasons. First, we have made the first detailed computational study of the docking of a series of diphosphates and a phosphonate to the isoprene biosynthesis pathway enzymes farnesyl diphosphate synthase, isopentenyl diphosphate/dimethylallyl diphosphate isomerase and deoxyxylulose-5-phosphate reductoisomerase. Overall, there is a 0.81 (±0.34) Å rms deviation between the docked and crystallographic structures, with the errors found being primarily a function of the number of ligand atoms present. Second, we have investigated the docking of the potent bisphosphonate drug, risedronate, to both a eukaryotic and a prokaryotic FPPS. The results show that the phosphonate moieties are involved in electrostatic interactions with Mg^{2+}, lysine and arginine, while the aromatic rings have both electrostatic (hydrogen bond) and hydrophobic interactions with other active site residues. Third, we investigated the docking of deoxyxylulose-5-phosphate to an NADPH−DXR complex. The docked DXP structure has a 0.90 Å heavy atom rms deviation from that found for fosmidomycin (in the X-ray structure of a fosmidomycin−DXR−Mn^{2+} complex) with O1 being 2.9 Å from H_s of NADPH. When taken together, these results demonstrate that the AutoDock procedure gives an excellent account of the docked structures of known phosphonate, bisphosphonate and diphosphate ligands bound to three isoprene biosynthesis pathway enzymes, which should enable its future use in the design of novel inhibitors of these important drug targets.

Acknowledgment. We thank D. Hosfield for providing the coordinates of PDB structures 1RQJ and 1RQI prior to PDB availability. This work was supported by the United States Public Health Service (NIH grant GM-65037).

References

(1) Rodan, G. A.; Martin, T. J. Therapeutic approaches to bone diseases. *Science* **2000**, *289*, 1508−1514.
(2) Miller, P. D. Efficacy and safety of long-term bisphosphonates in postmenopausal osteoporosis. *Expert. Opin. Pharmacother.* **2003**, *4*, 2253−2258.
(3) Rodriguez, N.; Bailey, B. N.; Martin, M. B.; Oldfield, E.; Urbina, J. A.; Docampo, R. Radical cure of experimental cutaneous leishmaniasis by the bisphosphonate pamidronate. *J. Infect. Dis.* **2002**, *186*, 138−140.
(4) Yardley, V.; Khan, A. A.; Martin, M. B.; Slifer, T. R.; Araujo, F. G.; Moreno, S. N.; Docampo, R.; Croft, S. L.; Oldfield, E. *In vivo* activities of farnesyl pyrophosphate synthase inhibitors against *Leishmania donovani* and *Toxoplasma gondii*. *Antimicrob. Agents. Chemother.* **2002**, *46*, 929−931.
(5) Das, H.; Wang, L.; Kamath, A.; Bukowski, J. F. Vγ2Vδ2 T-cell receptor-mediated recognition of aminobisphosphonates. *Blood* **2001**, *98*, 1616−1618.
(6) Wilhelm, M.; Kunzmann, V.; Eckstein, S.; Reimer, P.; Weissinger, F.; Ruediger, T.; Tony H. P. $\gamma\delta$ T cells for immune therapy of patients with lymphoid malignancies. *Blood* **2003**, *102*, 200−206.
(7) Wang, L.; Kamath, A.; Das, H.; Li, L.; Bukowski, J. F. Antibacterial effect of human Vγ2Vδ2 T cells *in vivo*. *J. Clin. Invest.* **2001**, *108*, 1349−1357.
(8) Lu, X. J.; Christensen, D. J.; Poulter, C. D. Isopentenyl-diphosphate isomerase: irreversible inhibition by 3-methyl-3,4-epoxybutyl diphosphate. *Biochemistry* **1992**, *31*, 9955−9960.
(9) Wouters, J.; Oudjama, Y.; Ghosh, S.; Stalon, V.; Droogmans, L.; Oldfield, E. Structure and mechanism of action of isopentenylpyrophosphate-dimethylallylpyrophosphate isomerase. *J. Am. Chem. Soc.* **2003**, *125*, 3198−3199.
(10) Wouters, J.; Oudjama, Y.; Barkley, S. J.; Tricot, C.; Stalon, V.; Droogmans, L.; Poulter, C. D. Catalytic mechanism of *Escherichia coli* isopentenyl diphosphate isomerase involves Cys-67, Glu-116, and Tyr-104 as suggested by crystal structures of complexes with transition state analogues and irreversible inhibitors. *J. Biol. Chem.* **2003**, *278*, 11903−11908.
(11) Jomaa, H.; Wiesner, J.; Sanderbrand, S.; Altincicek, B.; Weidemeyer, C.; Hintz, M.; Turbachova, I.; Eberl, M.; Zeidler, J.; Lichtenthaler, H. K.; Soldati, D.; Beck, E. Inhibitors of the nonmevalonate pathway of isoprenoid biosynthesis as antimalarial drugs. *Science* **1999**, *285*, 1573−1576.
(12) Wiesner, J.; Borrmann, S.; and Jomaa, H. Fosmidomycin for the treatment of malaria. *Parasitol. Res.* **2003**, *90*, S71−S76.
(13) Tarshis, L. C.; Proteau, P. J.; Kellogg, B. A.; Sacchettini, J. C.; Poulter, C. D. Regulation of product chain length by isoprenyl diphosphate synthases. *Proc. Natl. Acad. Sci. U.S.A.* **1996**, *93*, 15018−15023.

(14) Steinbacher, S.; Kaiser, J.; Eisenreich, W.; Huber, R.; Bacher, A.; Rohdich, F. Structural basis of fosmidomycin action revealed by the complex with 2-C-methyl-D-erythritol 4-phosphate synthase (IspC). Implications for the catalytic mechanism and antimalaria drug development. *J. Biol. Chem.* **2003**, *278*, 18401−18407.
(15) Hosfield, D. J.; Zhang, Y.; Dougan, D. R.; Broun, A.; Tari, L. W.; Swanson, R. V.; Finn, J. Structural basis for bisphosphonate-mediated inhibition of isoprenoid biosynthesis. *J. Biol. Chem.* **2004**, *279*, 8526−8529.
(16) Goodsell, D. S.; Morris, G. M.; Olson, A. J. Automated docking of flexible ligands: applications of AutoDock. *J. Mol. Recognit.* **1996**, *9*, 1−5.
(17) SYBYL 6.9, Tripos Inc., 1699 South Hanley Rd., St. Louis, MO 63144.
(18) Cornell, W. D.; Cieplak, P.; Bayly, C. I.; Gould, I. R.; Merz, Jr., K. M.; Ferguson, D. M.; Spellmeyer, D. C.; Fox, T.; Caldwell, J. W.; Kollman, P. A. A second generation force field for the simulation of proteins, nucleic acids, and organic molecules. *J. Am. Chem. Soc.* **1995**, *117*, 5179−5197.
(19) Gasteiger, J.; Marsili, M. Iterative partial equalization of orbital electronegativity − A rapid access to atomic charges. *Tetrahedron* **1980**, *36*, 3219−3288.
(20) Clark, M.; Cramer, R. D., III.; Van Opdenbosch, N. Validation of the general purpose Tripos 5.2 force field. *J. Comput. Chem.* **1989**, *10*, 982.
(21) PDB File 1PPW: Wouters, J.; Yin, F.; Song, Y.; Oudjama, Y.; Stalon, V.; Droogmans, L.; Kuzuyama, T.; Morita, C. T.; Oldfield, E., unpublished results.
(22) Yajima, S.; Nonaka, T.; Kuzuyama, T.; Seto, H.; Ohsawa, K. Crystal structure of 1-deoxy-D-xylulose 5-phosphate reductoisomerase complexed with cofactors: implications of a flexible loop movement upon substrate binding. *J. Biochem.* **2002**, *131*, 313−317.
(23) Wallace, A. C.; Laskowski, R. A.; Thornton, J. M. LIGPLOT: A program to generate schematic diagrams of protein−ligand interactions. *Protein Eng.* **1995**, *8*, 127−134.
(24) Dunford, J. E.; Thompson, K.; Coxon, F. P.; Luckman, S. P.; Hahn, F. M.; Poulter, C. D.; Ebetino, F. H.; Rogers, M. J. Structure−activity relationships for inhibition of farnesyl diphosphate synthase *in vitro* and inhibition of bone resorption *in vivo* by nitrogen-containing bisphosphonates. *J. Pharmacol. Exp. Ther.* **2001**, *296*, 235−242.
(25) Montalvetti, A.; Bailey, B. N.; Martin, M. B.; Severin, G. W.; Oldfield, E.; Docampo, R. Bisphosphonates are potent inhibitors of *Trypanosoma cruzi* farnesyl pyrophosphate synthase. *J. Biol. Chem.* **2001,** *276*, 33930−33937.
(26) Montalvetti, A.; Fernandez, A.; Sanders, J. M.; Ghosh, S.; Van Brussel, E.; Oldfield, E.; Docampo, R. Farnesyl pyrophosphate synthase is an essential enzyme in *Trypanosoma brucei*. *In vitro* RNA interference and *in vivo* inhibition studies. *J. Biol. Chem.* **2003**, *278*, 17075−17083.
(27) Sanders, J. M.; Gomez, A. O.; Mao, J.; Meints, G. A.; Van Brussel, E. M.; Burzynska, A.; Kafarski, P.; Gonzalez-Pacanowska, D.; Oldfield, E. 3-D QSAR investigations of the inhibition of *Leishmania major* farnesyl pyrophosphate synthase by bisphosphonates. *J. Med. Chem.* **2003**, *46*, 5171−5183.
(28) Keller, R. K.; Fliesler, S. J. Mechanism of aminobisphosphonate action: characterization of alendronate inhibition of the isoprenoid pathway. *Biochem. Biophys. Res. Commun.* **1999**, *266*, 560−563.
(29) Martin, M. B.; Sanders, J. M.; Kendrick, H.; de Luca-Fradley, K.; Lewis, J. C.; Grimley, J. S.; Van Brussel, E. M.; Olsen, J. R.; Meints, G. A.; Burzynska, A.; Kafarski, P.; Croft, S. L.; Oldfield, E. Activity of bisphosphonates against *Trypanosoma brucei rhodesiense*. *J. Med. Chem.* **2002**, *45*, 2904−2914.
(30) Kotsikorou, E.; Oldfield, E. A quantitative structure−activity relationship and pharmacophore modeling investigation of aryl-X and heterocyclic bisphosphonates as bone resorption agents. *J. Med. Chem.* **2003**, *46*, 2932−2944.
(31) Sanders, J. M.; Ghosh, S.; Chan, J. M. W.; Meints, G.; Wang, H.; Raker, A. M.; Song, Y.; Colantino, A.; Burzynska, A.; Kafarski, P.; Morita, C. T.; Oldfield, E. Quantitative structure−activity relationships for γδ T cell activation by bisphosphonates. *J. Med. Chem.* **2004**, *47*, 375−384.
(32) Gossman, W. L.; Wilson, S. R.; Oldfield, E. Three hydrates of the bisphosphonate risedronate, consisting of one molecular and two ionic structures. *Acta Crystallogr. C* **2003**, *59*, m33−m36.
(33) Martin, M. B.; Arnold, W.; Heath, H. T., III.; Urbina, J. A.; Oldfield, E. Nitrogen-containing bisphosphonates as carbocation transition state analogues for isoprenoid biosynthesis. *Biochem. Biophys. Res. Commun.* **1999**, *263*, 754−758.

JM040036S